ACS OMEGA

Open Access

This article is licensed under CC-BY-NC-ND 4.0

http://pubs.acs.org/journal/acsodf

Article

High-Efficiency Corrosion Inhibitor of Biomass-Derived High-Yield Carbon Quantum Dots for Q235 Carbon Steel in 1 M HCl Solution

Liming Dong, Yuyue Ma, Xiaohan Jin, Li Feng, Hailin Zhu, Zhiyong Hu, and Xuemei Ma*

Cite This: *ACS Omega* 2023, 8, 46934−46945

Read Online

ACCESS | Metrics & More | Article Recommendations | Supporting Information

ABSTRACT: Eco-friendly self-doped carbon quantum dots (ZCQDs) with excellent corrosion inhibition ability were prepared via solid-phase pyrolysis only using *Zanthoxylum bungeanum* leaves as the raw material. Compared with the relevant research, a simpler and higher yield (25%) preparation process for carbon quantum dots was proposed. ZCQDs were characterized by transmission electron microscopy and X-ray photoelectron spectroscopy, and the average size of ZCQDs with multitudes of O- and N-containing functional groups was about 2.53 nm. The prepared ZCQDs were used to inhibit the corrosion of Q235 steel in HCl solution, and the inhibition behavior was investigated through weight loss, electrochemical test, surface analysis, and adsorption thermodynamic analyses. The results showed that the ZCQDs, acted as a mixed corrosion inhibitor, have an effective corrosion inhibition for Q235, the corrosion inhibition efficiency reached 95.98% at 200 mg/L, and at this concentration, effective protection of at least 132h (IE > 90%) is provided. Moreover, the adsorption mechanism of ZCQDs was consistent with that of Redlich−Peterson adsorption, including chemisorption and physisorption. A new corrosion inhibition mechanism of ZCQDs has been thoroughly studied and proposed; ZCQDs have functional groups containing O and N, which can form a protective barrier through physical adsorption and chemisorption, but the coverage of the protective film is low at low concentrations. With the increase of concentration, the protective film formed by ZCQDs on the metal surface will first increase the coverage and then adsorb more ZCQDs on the protective film to form a thicker and denser protective film to protect the metal. The carbon quantum dots prepared in this paper have advantages including a green, renewable precursor, a fast method, high yield, and excellent corrosion inhibition. Therefore, this work can inspire and facilitate, to a certain extent, the future application of doped carbon quantum dots as efficient corrosion inhibitors in HCl solutions.

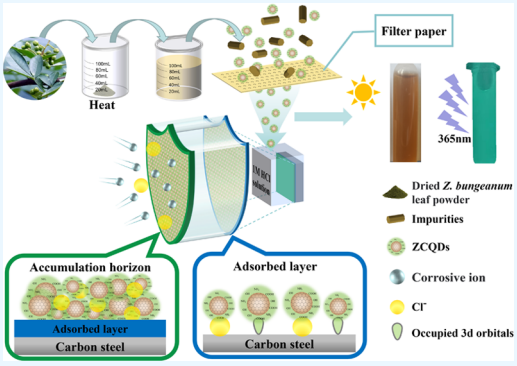

1. INTRODUCTION

Carbon steel is a kind of metal material that can be seen everywhere in daily life and industrial production.[1] Carbon steel in acidic environments will have serious corrosion, leading to serious safety accidents and huge economic losses.[2] Hence, different types of corrosion inhibitors are developed to inhibit corrosion in the industry. Highly effective corrosion inhibitors commonly used for carbon steel in acidic environments usually contain N, O, S, and other heteroatoms, aromatic rings, or heterocyclic compounds containing π-electrons, because these substances can form a protective film on the surface of carbon steel by forming coordination bonds (chemisorbing) and/or the electrostatic interaction between carbon steel and the corrosion inhibitor (physical adsorption).[3,4] However, with increasing concern for the ecological environment, many traditional corrosion inhibitors have been phased out due to their toxicity and difficulty in degradation. Therefore, it is of great significance to develop novel and efficient green corrosion inhibitors.

At present, a variety of green corrosion inhibitors have been developed, among which plant extracts and carbon dots (CDs) as corrosion inhibitors have attracted attention of many researchers. Plant extracts, as corrosion inhibitors, have advantages of low raw material cost, a wide range of sources, and renewability. However, plant extract corrosion inhibitors generally have problems, such as low corrosion inhibition efficiency (usually less than 90%), cumbersome extraction steps, and many toxic compounds used in preparation.[5,6] CDs are a zero-dimensional carbon-based nanomaterial, which is easy to modify, has good biocompatibility and excellent water solubility, and is widely used in the fields of photocatalysis/electrocatalysis, biological imaging, targeted drug carrier, and so on.[7,8] Therefore, compared with the traditional corrosion inhibitors, CDs as a corrosion inhibitor have an inherent safety advantage. In 2017, Cui et al. first reported that carbon dots could effectively inhibit metal corrosion in a 1 M hydrochloric

Received: September 5, 2023
Revised: November 1, 2023
Accepted: November 6, 2023
Published: November 17, 2023

© 2023 The Authors. Published by American Chemical Society

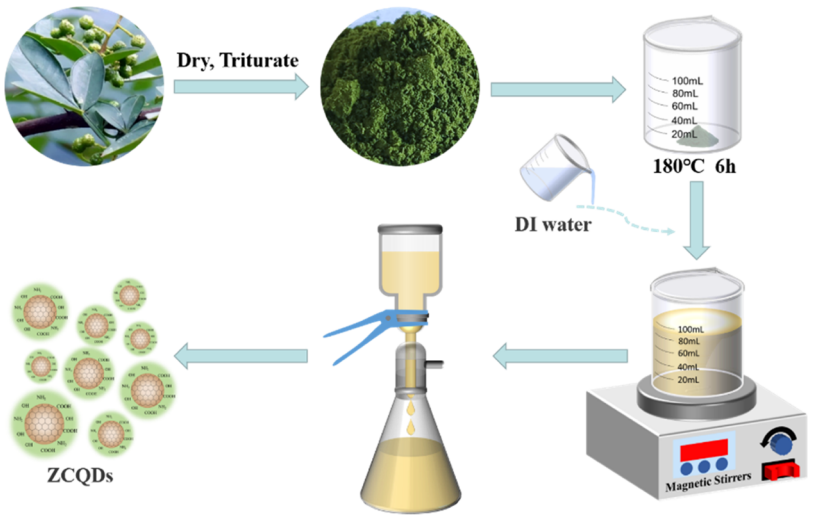

Figure 1. Diagram of the preparation of ZCQDs.

acid solution.[9] Since then, corrosion inhibitors for CDs have made great progress. The researchers found that doping N heteroatoms in CDs can improve the corrosion inhibition performance of CDs, and the corrosion inhibition rate of nitrogen-doped carbon dots (NCDs) is usually greater than 90% in an acidic environment; this is because N was doped into the CDs in the form of pyridine-like N, pyrrole-like N, or graphitic N, which improved the film formation of NCDs on the metal surface.[10−12] However, almost all of the efficient NCD inhibitors currently available are obtained by the hydrothermal method using small organic molecules as precursors.[13−15] Also, the separation and purification of CDs require high-speed centrifugation, filter membrane filtration, and membrane dialysis, and then vacuum drying and freeze-drying are performed. The dialysis and drying are very time-consuming and laborious, usually more than 48 h, and some even need more than 100 h. And the current yield of CD corrosion inhibitors is mostly less than 5%. This makes the synthesis and separation process of NCDs complex and costly, which limits its anticorrosion application. Noticeably, most reports point out that when CDs are used as a corrosion inhibitor, their adsorption mostly followed the Langmuir adsorption isotherm model.[16−18] However, carbon dots are corrosion inhibitors based on zero-dimensional nanomaterials, and their specific diffusion behavior and aggregation characteristics in corrosive media have not been studied deeply. Therefore, it is of great significance to establish a simple method for preparing carbon dots using biomass resources as raw materials and analyze its mechanism in the process of inhibiting corrosion. Zanthoxylum leaves are an agricultural waste, and their output is about 70 times that of *Zanthoxylum bungeanum*. Alkaloid and amides as N-containing ingredients are widely distributed in the leaves of *Z. bungeanum*, among which hydroxy-sanshool and long-chain unsaturated amide substances are the main numb-taste and pungent ingredients.[19,20] So, these ingredients may be used as self-dopants to obtain NCDs.[21] In order to make the product more suitable for industrial production, the solid-phase pyrolysis process, which is efficient and convenient and can produce carbon dots on a large scale, was selected.[22]

In this study, *Z. bungeanum* leaves, rich in alkaloids and amides, were used as precursors, and *Z. bungeanum* leaves carbon quantum dots (ZCQDs), capable of nitrogen atom self-doping, were prepared by the pyrolysis method. ZCQDs were characterized by thermogravimetric analysis (TGA), Raman spectroscopy, ultraviolet−visible spectroscopy (UV−vis), X-ray photoelectronic spectroscopy (XPS), transmission electron microscopy (TEM), and Fourier transform infrared (FTIR) spectroscopy. The corrosion inhibition characteristics were studied in detail by a weight loss test, potentiodynamic polarization (PDP), and electrochemical impedance spectroscopy (EIS). The surface analysis of carbon steel was performed using an atomic force microscope (AFM), a scanning electron microscope (SEM), and an energy-dispersive spectrometer (EDS). The corrosion inhibition mechanism of ZCQDs on Q235 carbon steel in 1 M HCl solution was analyzed by means of R−P adsorption isotherm, electrochemical analysis results, and metal surface morphology.

2. EXPERIMENTAL SECTION

2.1. Materials and Reagents. The Q235 carbon steel used for weight loss measurements and electrochemical tests was purchased locally and its composition ratio (wt %) was as follows: C, 0.19; Si, 0.31; Mn, 0.45; P, 0.02; S, 0.03; and Fe, remaining. In order to obtain more accurate weight loss tests, electrochemical tests, AFM, SEM, and EDS data, the surface of Q235 carbon steel sheet was polished with silicon carbide paper of different specifications ranging from 240 to 3000 mesh. After polishing, the surface was washed with DI water first and then degreased with ethanol; finally, the sample Q235 was slowly dried with cold air. HCl (AR 36−38%) used was purchased from Sinopharm Chemical Reagent Co. All of the water used in the experiment was DI water made by the laboratory. The *Z. bungeanum* leaves were collected from Yangqu County, Shanxi Province, China, in August 2021.

2.2. Synthesis of *Z. bungeanum* Leaf-Derived CQDs (ZCQDs). The *Z. bungeanum* leaf-derived CDs (ZCQDs) were synthesized by the solid-phase pyrolysis method, as shown in Figure 1. First, 10 g of dried and crushed *Z. bungeanum* leaves were placed in a beaker and heated at a constant temperature for 6 h in a drying oven at 180 °C. After natural cooling to room temperature, ultrapure water was added to a beaker for stirring. Then, the ordinary medium-speed filter paper and 0.22 μm filter membrane were used successively to filter, and the large particles insoluble in water such as residual leaves were

https://doi.org/10.1021/acsomega.3c06702
ACS Omega 2023, 8, 46934−46945

Table 1. Corrosion Rate of Q235 Carbon Steel and Inhibition Efficiency (η) of ZCQDs in 1 M HCl with Various Contents

content (mg/L)	long (mm)	wide (mm)	high (mm)	Φ (mm)	A (m^2)	W_0 (g)	W (g)	corrosion rate ($g \cdot cm^{-2} \cdot h^{-1}$)	η (%)
0	25	25	2.8000	3	0.001530	13.2637	12.3415	25.1144	
50	25	25	2.8000	3	0.001530	13.6667	13.3735	7.9963	68.16
100	25	25	2.7667	3	0.001527	13.5432	13.4466	2.6365	89.50
150	25	25	2.7000	3	0.001520	13.1901	13.1288	1.6813	93.31
200	25	25	2.7500	3	0.001530	13.2388	13.1980	1.1157	95.56

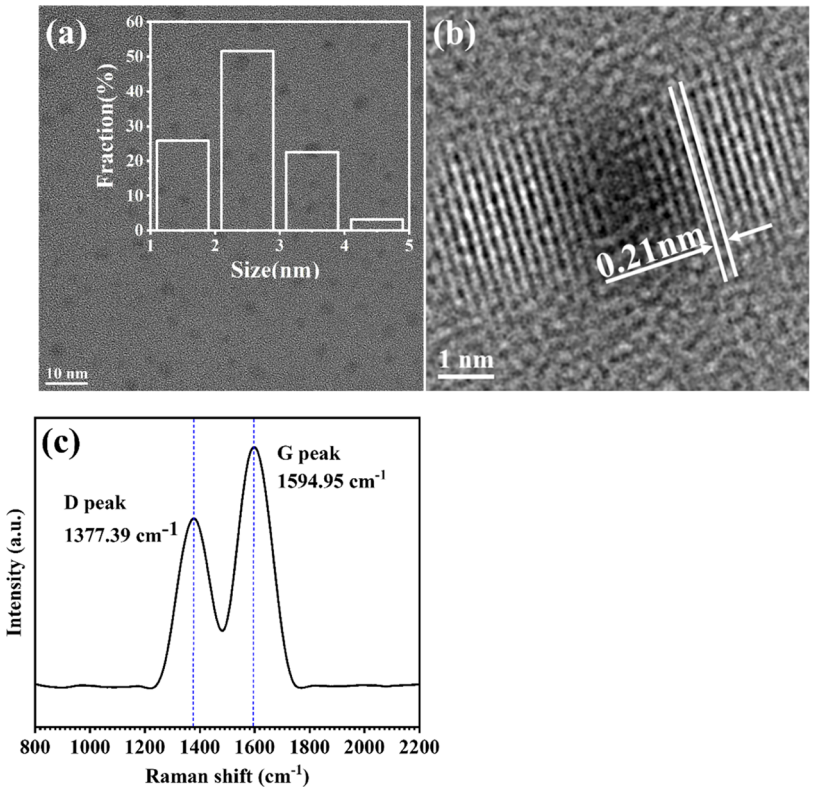

Figure 2. (a) TEM (with a size distribution, inset) and (b) HRTEM images of ZCQDs. (c) Raman spectrum.

removed. It is exciting that the yield of ZCQDs prepared by this method can reach more than 25%, which is much higher than that reported by existing CQD corrosion inhibitors, and the speed is faster and the operation is simpler.

2.3. Characterization of ZCQDs. The morphology, particle size distribution, and lattice spacing of ZCQDs were obtained by TEM (FEI Talos F200X G2). In order to further understand the fine structure of ZCQDs, Raman spectroscopy (Horiba LabRAM HR Evolution, Japan) was used to record the data of 800−2200 cm^{-1} at a laser wavelength of 532 nm and analyze the degree of graphitization. The FTIR spectra (Thermo Fisher Nicolet iS50) of 600−4000 cm^{-1} were obtained using a diffuse infrared technique, and the data of 200−700 nm were recorded using a UV−vis spectrometer (PerkinElmer Lambda 35) for the analysis of functional groups of ZCQDs. The data of ZCQDs at 30−650 °C were obtained by TG (Mettler Toledo TGA 1, Switzerland), and the fine structure of ZCQDs was analyzed by XPS (Thermo Scientific K-Alpha). The ζ-potential of ZCQDs in 1 M HCl solution was tested using an ζ-potential analyzer (Brookhaven).

2.4. Weight Loss Measurements. The sample size of Q235 carbon steel for the weight loss test is shown in Table 1. The sample was soaked in 1 M HCl solution without ZCQDs and with different amounts of ZCQDs for 24 h. The weighing accuracy before and after the experiment was 0.1 mg, and weighing was carried out three times to take an average value. The vessel used for the weight loss measurement experiment was a 100 mL jacketed beaker, and the temperature was maintained at 25 °C during the experiment.

2.5. Electrochemical Measurements. Electrochemical test scheme: ZCQDs were directly dissolved in 1 M HCl to produce HCl solutions containing 50, 100, 150, and 200 mg/L ZCQDs. Electrochemical measurements were performed in the produced inhibited solutions using a three-electrode system on an electrochemical workstation (CS2350M, CORRTEST, China). A saturated calomel electrode (reference electrode), a platinum sheet (counter electrode), and a Q235 carbon steel coupon enwrapped in epoxy resin with only one exposed surface of 1.0 cm × 1.0 cm comprised the three-electrode system (working electrode).[23,24] The open-circuit potential should reach a stable state before the EIS and DPP tests. The electrochemical impedance was measured at a scanning frequency of 10 mV/s in the range of 10^5−10^{-2} Hz, and the impedance data were fitted and analyzed using ZSimpWin. The action potential polarization test was performed at a rate of 0.5 mV/s within the range of ±250 mV.[25,26] All electrochemical tests were repeated three times to ensure data repeatability.

2.6. Surface Characterization. After the weight loss experiment, the sample of Q235 carbon steel used in the

https://doi.org/10.1021/acsomega.3c06702
ACS Omega 2023, 8, 46934−46945

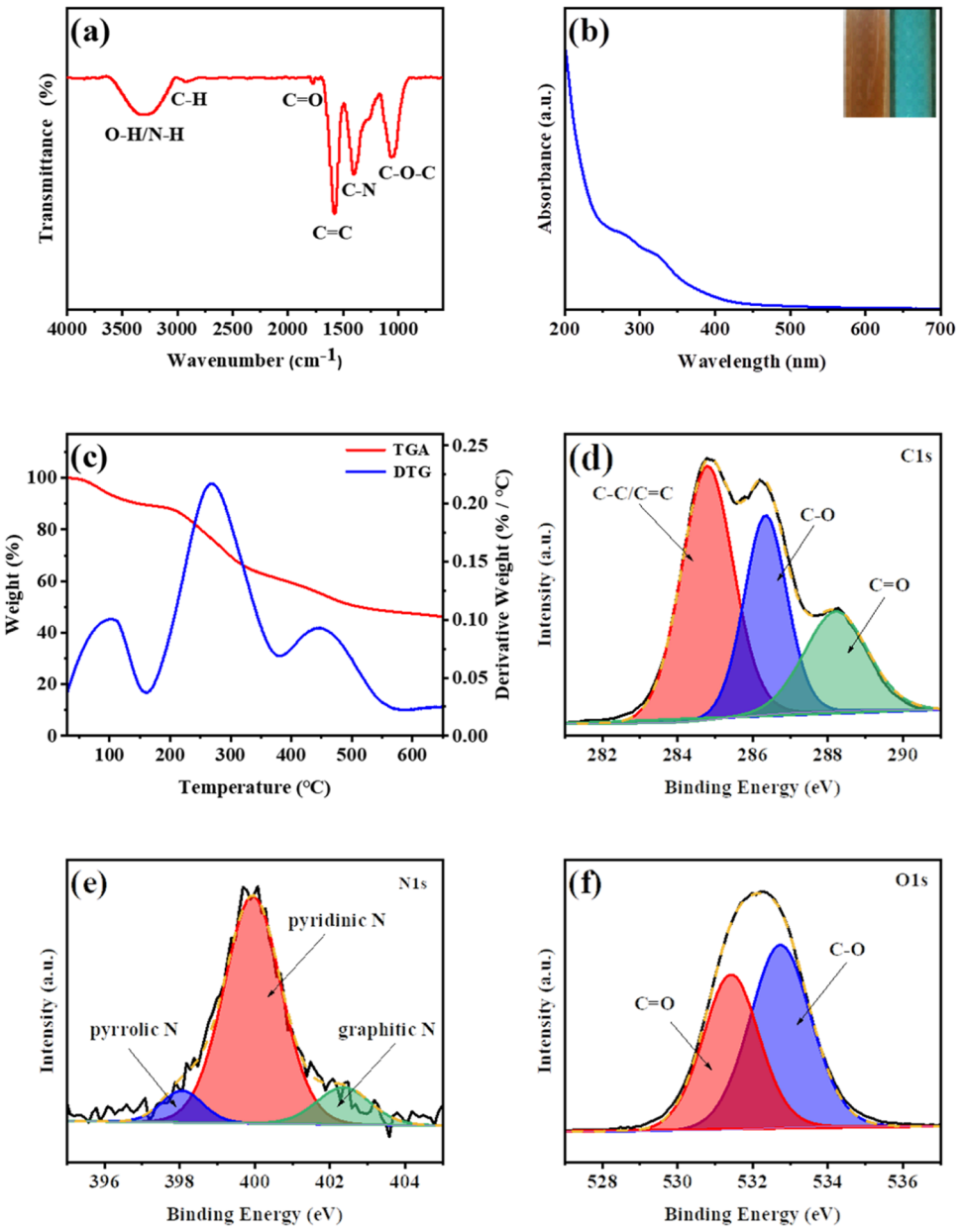

Figure 3. (a) FTIR spectra and (b) UV−vis absorption spectra. Inset: Pictures of the ZCQDs under daylight (left) and UV light (365 nm) (right). (c) Thermogravimetric analysis (TGA: red curve) and derivative thermogravimetric analysis (DTG: blue curve) thermograms of ZCQDs; (d−f) XPS survey, C 1s, N 1s, and O 1s spectra of ZCQDs.

experiment was taken out, washed with DI water, and then slowly dried in dry cold air. Atomic force microscopy (Bruker Dimension Icon, Germany) and scanning electron microscopy (TESCAN MIRA LMS, Czech Republic) were used to analyze two-dimensional and three-dimensional structures on the surface of carbon steel. The components of the metal surface elements in different states were analyzed by EDS.

3. RESULTS AND DISCUSSION

3.1. Characterization of ZCQDs. The size and structure of ZCQDs were analyzed by TEM observation. 100 ZCQDs were randomly selected, and their sizes were statistically analyzed. The obtained data are shown in the table inset in Figure 2a. The average size of ZCQDs is about 2.53 nm, with most sizes between 2 and 3 nm, and their shape is spheroid. Figure 2b shows a high-resolution image of ZCQDs. Digital micrograph analysis shows that the lattice spacing is 0.21 nm (Figure S1). This result is consistent with the (1 0 0) face of graphene, which proves that ZCQDs are mainly graphene structures.[27−29] According to Raman spectroscopy (Figure 2c), peak D caused by disorderly vibration of graphene, which can reflect graphene defects, and peak G caused by in-plane vibration of the sp^2 carbon atom, which can reflect the thickness of the graphene material, are at 1337.39 and 1594.95 cm^{-1}, respectively, in ZCQDs.[27,30] The ratio of peak D to peak G intensity can be used to obtain the degree of disorder of graphitic carbon, and the ID/IG value can be obtained by calculation as 0.86. Therefore, it can be seen that the degree of graphitization of ZCQDs is good, which is mainly stacked by sp^2 hybrid carbon.[28] In conclusion, ZCQDs are carbonized by cross-linking polymerization of various components in *Z.*

https://doi.org/10.1021/acsomega.3c06702
ACS Omega 2023, 8, 46934−46945

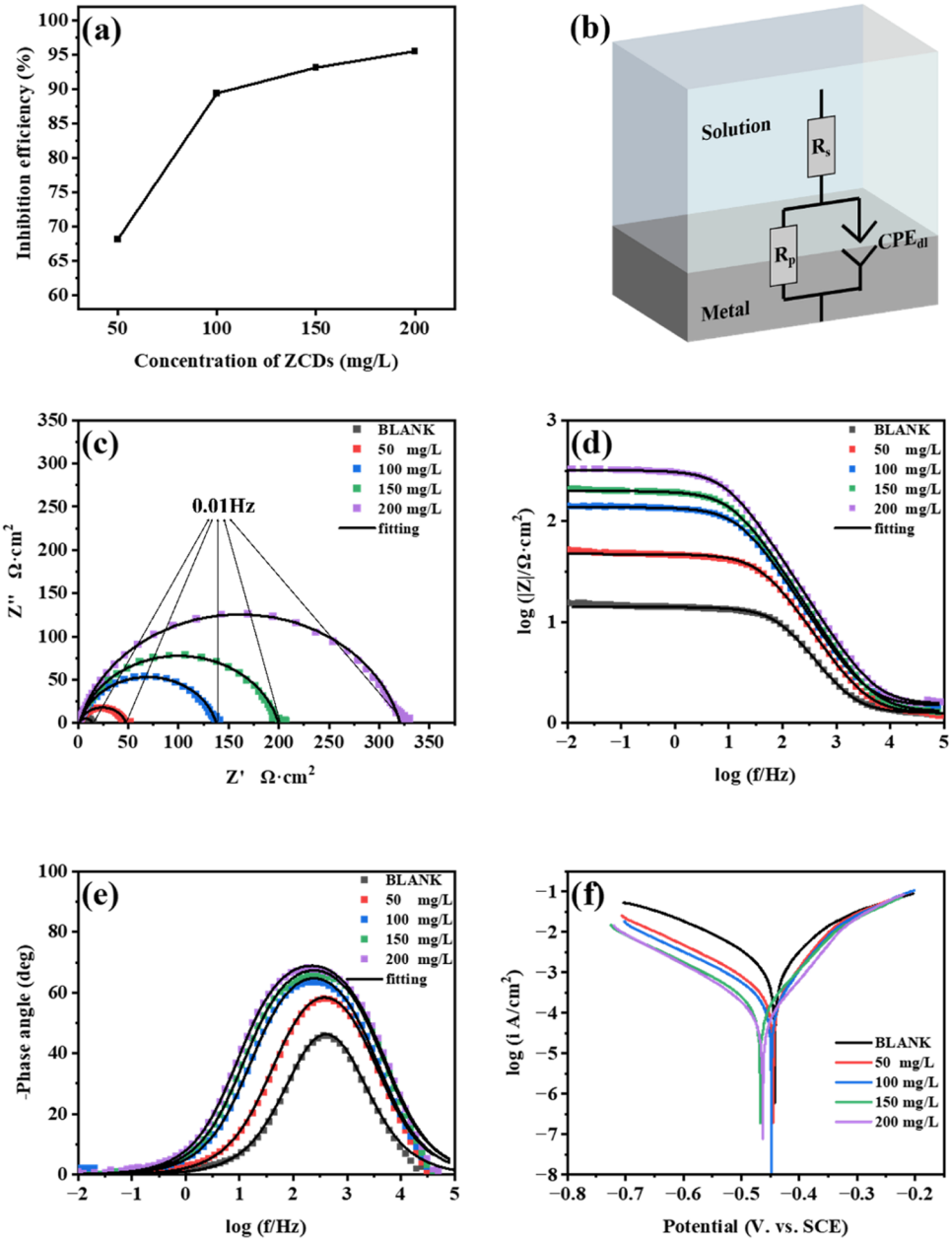

Figure 4. (a) Inhibition rates of different concentrations of ZCQDs after being soaked for 24 h. (b) Electrical equivalent circuit fitted by EIS data. Electrochemical characterizations of (c) Nyquist plot, (d, e) Bode plot, and (f) PDP.

bungeanum leaves at high temperatures to form carbon quantum dots with sp^2 hybrid carbon as the core.

Figure 3a shows the Fourier transform infrared spectra of the ZCQDs. In the figure, the peak at 3423 cm^{-1} is caused by the tensile vibration of O−H/N−H, and the peak at 2930 cm^{-1} is caused by C−H. The four peaks of 1770 cm^{-1}, 1575 cm^{-1}, 1404, and 1043 cm^{-1} correspond to C−H, C═O/C═C, C−N, and C−O−C,[29,31] respectively. Figure 3b shows the UV−vis absorption spectra of ZCQDs in the 200−700 nm range. It can be seen from the figure that ZCQDs have two peaks at 275 and 325 nm, which are caused by the $\pi \rightarrow \pi^*$ transition of electrons in the aromatic structure region and $n \rightarrow \pi^*$ transition of the aromatic sp^2 system containing C═O and C═N bonds, respectively.[29] The FTIR and UV−vis results show that ZCQDs contain rich functional groups, among which the one containing N proves that ZCQDs realize self-doping. As further proof of this conclusion, a thermodynamical analysis of ZCQDs was performed; the results are shown in Figure 3c, where the red line is the TGA mass loss curve, and the blue line is the DTG curve. The results show that ZCQDs have three weight losses at 80, 190, and 365 °C, respectively. Comprehensive analysis shows that when the temperature is between 80 and 160 °C, the first degradation of ZCQDs is due to the heat loss of adsorbed free water, crystal water, and bonding water on ZCQDs, and the second degradation occurs between 190 and 360 °C, which is due to the thermal decomposition of amide, hydroxyl, and some unsaturated double bonds on ZCQDs. The final degradation occurs between 390 and 590 °C, and the mass loss in this stage is caused by the carbonization of organic matter remaining in the previous degradation stage.[27−29] Based on the above results, it can be seen that ZCQDs achieve self-doping. In order to

https://doi.org/10.1021/acsomega.3c06702
ACS Omega 2023, 8, 46934−46945

Table 2. Fitting Parameters of Q235 Carbon Steel in Various Solutions

content (mg/L)	R_S (Ω cm^2)	R_P (Ω cm^2)	C_{dl} (μF cm^{-2})	$Y_0 \times 10^{-6}$ (Ss^n cm^{-2})	n	IE_{EIS} (%)
0	1.246	12.88	1448.217864	331.3	0.85	
50	1.238	45.19	968.4861944	185.4	0.8453	71.50
100	1.475	136.2	904.1696045	145.6	0.8442	90.54
150	1.292	198.7	807.8734317	127.4	0.8459	93.52
200	1.532	320.6	642.7881856	97.3	0.8457	95.98

further explore the fine structure of ZCQDs, we characterized them with XPS. The full spectrum of XPS (Figure S2) shows that ZCQDs have three characteristic peaks at 284, 399, and 531 eV, corresponding to C 1s, N 1s, and O 1s, respectively. By software analysis, the relative contents of C atom, O atom, and N atom in the surface layer of ZCQDs are 59.53, 38.11, and 2.36%, respectively. Figure 3d shows the high-resolution spectrum of C 1s; it can be clearly seen that C−C/C═C, C−O, and C═O correspond to three different types of C at 284.8, 286.4, and 288.2 eV, respectively. Figure 3e shows the high-resolution spectrum of N 1s, showing that N exists in ZCQDs in three forms, namely, pyrrole N (398.06 eV), pyridine N (399.95 eV), and graphite N (402.36 eV). In the high-resolution spectrum of O 1s (Figure 3f), two characteristic peaks representing C═O and C−O appear at 531.42 and 532.74 eV.[32] The results of FTIR, UV−vis, TG, and XPS were in good agreement. These data strongly prove that solid-phase pyrolysis can self-dope N in *Z. bungeanum* leaves to form ZCQDs containing N groups.

3.2. Corrosion Inhibition Characteristics. *3.2.1. Weight Loss Analysis.* Figure 4a shows the corrosion rate of Q235 carbon steel in 1 M HCl solution without ZCQDs and with different concentrations of ZCQDs and the corrosion inhibition rate of ZCQDs on Q235 carbon steel. Specific parameters are given in Table 1.

The corrosion rate (V) and inhibition efficiency (IE_w%) were calculated according to the eqs 1 and 2:[25]

$$V = \frac{W_0 - W}{At} \tag{1}$$

$$IE_w = \frac{V_0 - V}{V_0} \times 100\% \tag{2}$$

In formulas 1 and 2, W_0 is the weight of Q235 carbon steel before the test, W is the weight after the test, A is the surface area of the test specimen, t is the soaking time, V_0 is the corrosion rate of Q235 carbon steel soaked in the 1 M HCl solution without adding ZCQDs, and V is the corrosion rate after adding ZCQDs.

Compared to the 1 M HCL solution without ZCQDs, the corrosion rate decreases significantly after the addition of ZCQDs, and the corrosion rate decreases with an increasing amount of ZCQDs, with the inhibition efficiency (IE_w%) proportional to the amount of ZCQDs. When the concentration is 200 mg/L, the inhibition efficiency (IE_w%) reaches 95.56%, and the corrosion rate of Q235 decreases by 95.58% (25.11−1.11 g·m^{-2}·h^{-1}) compared to soaking in 1 M HCl solution without adding ZCQDs. It is important to note that the growth of the inhibition efficiency of ZCQDs gradually slows down when the dosage reaches 100 mg/L. It is clear from the results of the weight loss experiment that the ZCQDs protect the carbon steel well in the 1 M HCl solution.

3.2.2. Electrochemical Impedance Spectroscopy Analysis. Figure 4c is a Nyquist plot and shows that the capacitive arc diameter increases significantly when ZCQDs are added to the HCl solution, indicating that ZCQDs can form a protective film on the metal surface. The addition of ZCQDs is proportional to the diameter, suggesting that increasing the addition of ZCQDs increases the thickness or coverage of the film. This protective film can reduce the area of the active reaction site on the metal surface and block the transfer of charge, thus inhibiting the corrosion of Q235 carbon steel in 1 M HCl solution.[15,33] The value of |Z| in the low-frequency region can also reflect the corrosion suppression performance of the corrosion suppressor. When Q235 carbon steel is in the blank solution without ZCQDs, the value of $|Z|_{0.01\ Hz}$ is about 14.13 Ω·cm^2. After the ZCQDs were added to the 1 M HCl solution, the value of |Z| increases with the addition amount. When the concentration is 200 mg/L, the value at $|Z|_{0.01\ Hz}$ reaches 320.28 Ω·cm^2, which is 22.67 times that of the blank solution. In Figure 4d, it can be clearly observed that log |Z| increases from 1.15 to 2.51 in the low-frequency region (0.01 Hz). The phase angle diagram (Figure 4e) shows that as the amount of added ZCQDs increases, the peak phase angle moves in a more negative direction, indicating that the protective film formed becomes denser as the concentration of ZCQDs increases.[34] Moreover, Figure 4e shows that with the increase of ZCQD concentration, the corresponding maximum phase angle frequency decreases, which may be due to the increase in the coverage and densification of the film formed by ZCQDs on the metal surface.[35−37] However, it is worth noting that whether ZCQDs are added or not, the phase angle diagram has only one peak, that is, the corrosion process has only one time constant, and the addition of ZCQDs will not affect the corrosion reaction process.[27,38] These data strongly prove that ZCQDs can form a protective layer on the metal surface.[39]

To better understand and fit the EIS data, an equivalent circuit is used as shown in Figure 4b, where R_s represents the resistance of the solution, R_p represents the polarization resistance, and CPEDL is the phase angle element used to represent the nonideal capacitance in the circuit. The detailed fit to the data is shown in Table 2. CPE is used to represent the phase angle element of the nonideal capacitance, which can be determined by eq 3:[40,41]

$$Z_{CPE} = \frac{1}{Y_0(i\omega)^n} \tag{3}$$

In eq 3, Y_0, ω, i, and n, respectively, represent the size, angular frequency, imaginary number unit, and ideal state of CPE. When n is −1, 0, and 1, CPE stands for inductance, resistance, and capacitance, respectively. When n is between −1 and 1, this is a nonideal capacitive or inductive behavior. Table 2 shows that n fluctuates around 0.845, which is mainly caused by the electrode surface state. The double-layer capacitance (C_{dl}) can be analyzed by eq 4[42]

$$C_{dl} = Y_0(2\pi f_{max})^{n-1} \tag{4}$$

https://doi.org/10.1021/acsomega.3c06702
ACS Omega 2023, 8, 46934−46945

Table 3. Electrochemical Parameters Obtained from PDP

content (mg/L)	E_{corr} (mV/SCE)	i_{corr} (μA/cm^2)	β_a (mV dec^{-1})	β_c (mV dec^{-1})	IE (%)
0	−0.44241	1845.8	121.42	−158.6	
50	−0.44481	414.39	84.349	−147.72	0.7755
100	−0.44813	306.53	81.379	−149.11	0.83393
150	−0.46715	190.89	81.882	−137.28	0.8966
200	−0.46285	98.114	71.095	−114.83	0.9468

where Y_0 is the magnitude of the C_{dl}, f_{max} is the frequency at the largest imaginary part of the impedance, and n can be considered as the surface roughness of the carbon steel. It is not difficult to find the trend of fluctuations in the n values from Table 2. The value of n decreases with the addition of ZCQDs. This is because the protective film formed by ZCQDs on the metal surface is not homogeneous and thus increases the roughness of the metal surface (compared to the metal surface in the original state). Therefore, the value of n can reflect whether ZCQDs as corrosion inhibitors can form a protective film on the metal surface to a certain extent. The value of C_{dl} can also be calculated and derived by the Helmholtz model equation shown in eq 5.[10,40]

$$C_{dl} = \frac{\varepsilon \times \varepsilon^0 \times S}{d} \tag{5}$$

wherein ε denotes the permittivity, ε^0 denotes the vacuum permittivity, S is the effective area of the electrode, and d represents the thickness. It can be clearly seen from the formula that C_{dl} is inversely proportional to d. Therefore, it can be inferred from the data in Table 2 that C_{dl} decreases with the increase in the addition amount of ZCQDs, and the thickness of the protective film formed by ZCQDs on the metal surface keeps increasing. The rate of corrosion suppression increases continuously as the thickness of the protective layer increases. Corrosion inhibition rate (IE_{EIS}) can be obtained by eq 6.[43]

$$IE_{EIS} = \frac{R_p - R_{p0}}{R_p} \times 100\% \tag{6}$$

In the formula, R_{p0} is the resistance without adding ZCQDs and R_p is the resistance after adding ZCQDs. The value of IE_{EIS} can be obtained by calculation. The resulting data are shown in Table 2. When the dosage reaches 200 mg/L, the IE_{EIS} value reaches 95.98%, and at this concentration, effective protection of at least 132h (IE > 90%) is provided (Figure S3 and Table S1). This indicates that ZCQDs can provide effective protection against Q235 carbon steel in a 1 M HCl solution. In addition, when the concentration reached 100 mg/L, the continued addition of ZCQDs could further improve the corrosion inhibition rate, but the growth rate gradually slowed down, which is consistent with the data of the weight loss experiment. It is also worth noting that the IE_{EIS} value is more than 90% when the dosage reaches 100 mg/L, indicating that ZCQDs can provide effective protection for the metal even at low concentrations.

3.2.3. Potentiodynamic Polarization (PDP) Analysis. Figure 4f depicts the PDP curve of Q235 steel in a 1 M HCl solution with and without the corrosion inhibitor ZCQDs. In the meantime, Table 3 provides a list of the pertinent PDP curve parameters.

Corrosion potential and current density are denoted by E_{corr} and i_{corr}, respectively. β_a and β_c are the relative slopes of the anodic and cathodic polarization curves tangential to the crossing point, respectively. IE_{PDP} represents the effectiveness of corrosion inhibition. Among them, IE_{PDP} value can be obtained from eq 7.[44]

$$IE_{PDP} = \frac{i_{corr}^0 - i_{corr}}{i_{corr}} \times 100\% \tag{7}$$

where i_{corr}^0 and i_{corr} are the corrosion rates without and with the inhibitor, respectively. Potentiodynamic polarization results are shown in Figure 4f and Table 3. With the increase in ZCQD concentration, the corrosion current will decrease. Both the cathode and anode showed a downward trend. After adding ZCQDs, the corrosion potential has a negative shift, and the higher the concentration of ZCQDs, the more obvious the shift. However, the displacement of the potential is not as drastic as that of the cathode inhibitor, and the maximum displacement is 25 mV compared with the Tafel data in the HCl solution without ZCQDs. When the corrosion potential change of the corrosion inhibitor is greater than 85 mV, the corrosion inhibitor is considered to be a cathode or anode corrosion inhibitor, and when the corrosion potential is less than 85 mV, the corrosion inhibitor is considered to be a mixed corrosion inhibitor, so ZCQDs should be a mixed corrosion inhibitor.[45,46] In Figure 4f, when the concentration of ZCQDs does not exceed 150 mg/L, the anode curve almost coincides, which corresponds to the value of β_a in Table 3. In this concentration range, the change of β_c is greater than that of β_a, which indicates that the main inhibition is cathodic corrosion at this time, and the addition of ZCQDs hinders the occurrence of the hydrogen evolution reaction. When the concentration reaches 200 mg/L, the cathodic protection continues to improve while the anode protection is also improved, which may be due to the increased thickness of ZCQDs deposited on the metal surface, causing the active site blocking effect and inhibiting the dissolution of metal in HCl.[34,47] This makes ZCQDs better protect the anode while protecting the cathode, which is why the corrosion potential at 200 mg/L will shift to the anode at about 0.05 mV compared to the corrosion potential at 150 mg/L. However, overall, ZCQDs are more focused on protecting the cathode. Therefore, ZCQDs are a hybrid corrosion inhibitor that focuses more on protecting the cathode. However, it is worth noting that whether ZCQDs are added or not, the phase angle diagram has only one peak, that is, the corrosion process has only one time constant, and the addition of ZCQDs will not affect the corrosion reaction process.[48,49] These data strongly prove that ZCQDs can form a protective layer on the metal surface. With the increase in ZCQDs, i_{corr} decreases rapidly, while IE_{PDP} increases rapidly. After the addition of 200 mg/L ZCQDs, IE_{PDP} can reach 94.68%, which is consistent with the results of weight loss measurements and EIS.

3.3. Adsorption Isotherm and Thermodynamic Analyses. The adsorption process is very important for the study of corrosion inhibitors. Common models, such as Langmuir, Temkin, and Freundlich adsorption isotherm

https://doi.org/10.1021/acsomega.3c06702
ACS Omega 2023, 8, 46934−46945

models, have been widely used in the study of the adsorption behavior of different corrosion inhibitors.[50,51] At present, some research on CD corrosion inhibitors directly use these equations, and the accuracy value obtained is also high. However, taking Langmuir, which is used most, as an example, adsorption with a monolayer should be used more. However, when studying the adsorption of CDs as corrosion inhibitors, we should pay attention to the heterogeneity caused by its own structure. These all have an effect on the adsorption process. Redlich−Peterson (R−P) adsorption isotherm equation is an adsorption model with three parameters. The R−P equation also contains features of the Langmuir and Freundlich models, but the R−P equation is modified by two parameters, such that the adsorption process of heterogeneous layers can be described more accurately than the Langmuir and Freundlich isotherm equations.[52] Therefore, the R−P equation can better reflect the adsorption process of CDs as a corrosion inhibitor. The R−P isotherm equation is expressed as in eq 8:

$$q_e = \frac{K_{RP}C_e}{1 + B_{RP}C_e^{\alpha}} \tag{8}$$

where K_{RP}, B_{RP}, and α are the three parameters in the R−P equation. In the adsorption process of nanoparticles as corrosion inhibitors, the value of α can be used to infer whether the adsorption type is monolayer adsorption or heterogeneous adsorption. The more α value approaches 1, the more similar it is to monolayer adsorption.[53] When the nonuniformity of the metal surface is ignored and it is regarded as an ideal solid surface, the influence of the nanoparticle structure on its effective corrosion inhibition concentration due to its agglomeration effect can be judged by the value of α, that is, the closer the α is to 1, the smaller the influence on the effective corrosion inhibition concentration.[28] Therefore, eq 9 can be obtained by transformation:

$$C_e^{\alpha} = \frac{K_{RP}C_e}{B_{RP}q_e} - \frac{1}{B_{RP}} \tag{9}$$

Ideally, surface coverage θ can be used as a reference to evaluate the adsorption quantity on the metal surface.[54] θ is presented as follows:

$$\theta = \frac{IE_{EIS}}{100} \tag{10}$$

The value of IE_{EIS} can be obtained by eq 6. Excel and Origin were used to calculate and fit the obtained data, and the best α value (α = 1.19) was obtained. The value of C_e^{α} was obtained by substituting the α value into C_e^{α}. The linear regression graph of C_e/q_e vs C_e^{α} was drawn (Figure 5), and the R^2 value reached 0.9993, which was significantly better than the R^2 value obtained by Freundlich's fitting (Figure S4a) and slightly better than the R^2 value obtained by Langmuir (Figure S4b). The comparison results show that the R−P equation is more suitable for the adsorption of CQD corrosion inhibitor on the metal surface. The better fitting results also indicate that the adsorption of ZCQDs on the metal surface should be a composite process of physical adsorption and chemical adsorption.[28,55] The α value close to 1 indicates that the adsorption of ZCQDs on the metal surface tends to be monolayer adsorption, which is why the Langmuir model can obtain relatively good fitting results (Figure S4b). However, ZCQDs belong to nanoparticles and have an inevitable nanoagglomeration effect, so the α value obtained by any

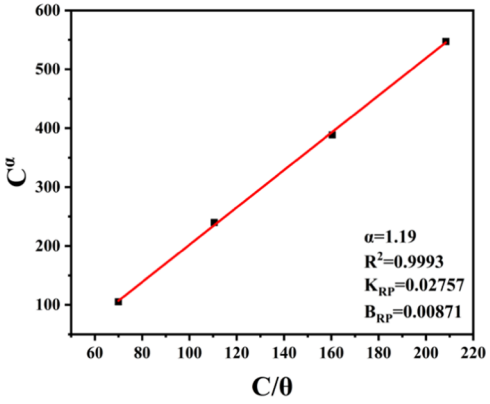

Figure 5. Adsorption isotherm plots of ZCQDs fitted with the Redlich−Peterson equation.

data is not equal to 1. At this time, if the nonuniformity of the metal surface is ignored and the value of α approaches 1, it can be inferred that the adsorption of ZCQDs on the metal surface is close to uniform adsorption, and the influence of its own structure is small.

3.4. Corrosion Morphology Analyses. In order to better understand the corrosion inhibition mechanism of ZCQDs, the corrosion morphology of Q235 carbon steel in the original state and the corrosion morphology of 1 M HCl without adding ZCQDs or adding 200 mg/L ZCQDs were analyzed by using AFM, SEM, and EDS. The three-dimensional topographies of the three states were obtained by AFM (Figure 6a−c). In the original state (Figure 6a), the surface of the metal was smooth, with only scratches and no large fluctuations. The roughness of the metal surface was analyzed by NanoScope Analysis 1.7 and R_a = 77 nm was obtained. When the metal was soaked in HCl solution without ZCQDs (Figure 6b), the metal surface fluctuated up to 4 μm and deep pits and accumulated corrosion products appeared. At this time, the roughness R_a = 377 nm. After ZCQDs were added to the solution, the surface of Q235 soaked for 24 h was significantly smoother than that of Q235 soaked in the solution without ZCQDs (Figure 6c), and the deep pit is almost invisible. Although the roughness R_a = 121 nm is slightly larger than the original state, it is far smaller than the roughness of the metal surface soaked in a blank HCl solution; the result that the roughness of the metal surface after adding ZCQDs is larger than that of the original state is also consistent with the results of EIS analysis. The height of the metal surface at this time is larger than the original state, which is due to the stack of ZCQDs on the carbon steel surface. It forms a thick protective layer. The results show that ZCQDs can effectively inhibit the corrosion rate of Q235 carbon steel in 1 M HCl, which is further verified by SEM images. As shown in Figure 6d−f, only scratches existed on the metal surface in the original state (Figure 6d). In the HCl solution without ZCQDs, the metal surface is severely corroded and a large number of corrosion products can be seen (Figure 6e). In the HCl solution containing 200 mg/L ZCQDs, a film appeared on the metal surface (Figure 6f), which was smoother than that soaked in the HCl solution without ZCQDs. The results of atomic force microscopy (AFM) and scanning electron microscopy (SEM) show that ZCQDs can form a thick protective film on the surface of carbon steel, thereby slowing down the corrosion of metal. In order to verify the above conclusion, the composition of metal surface elements in

https://doi.org/10.1021/acsomega.3c06702
ACS Omega 2023, 8, 46934−46945

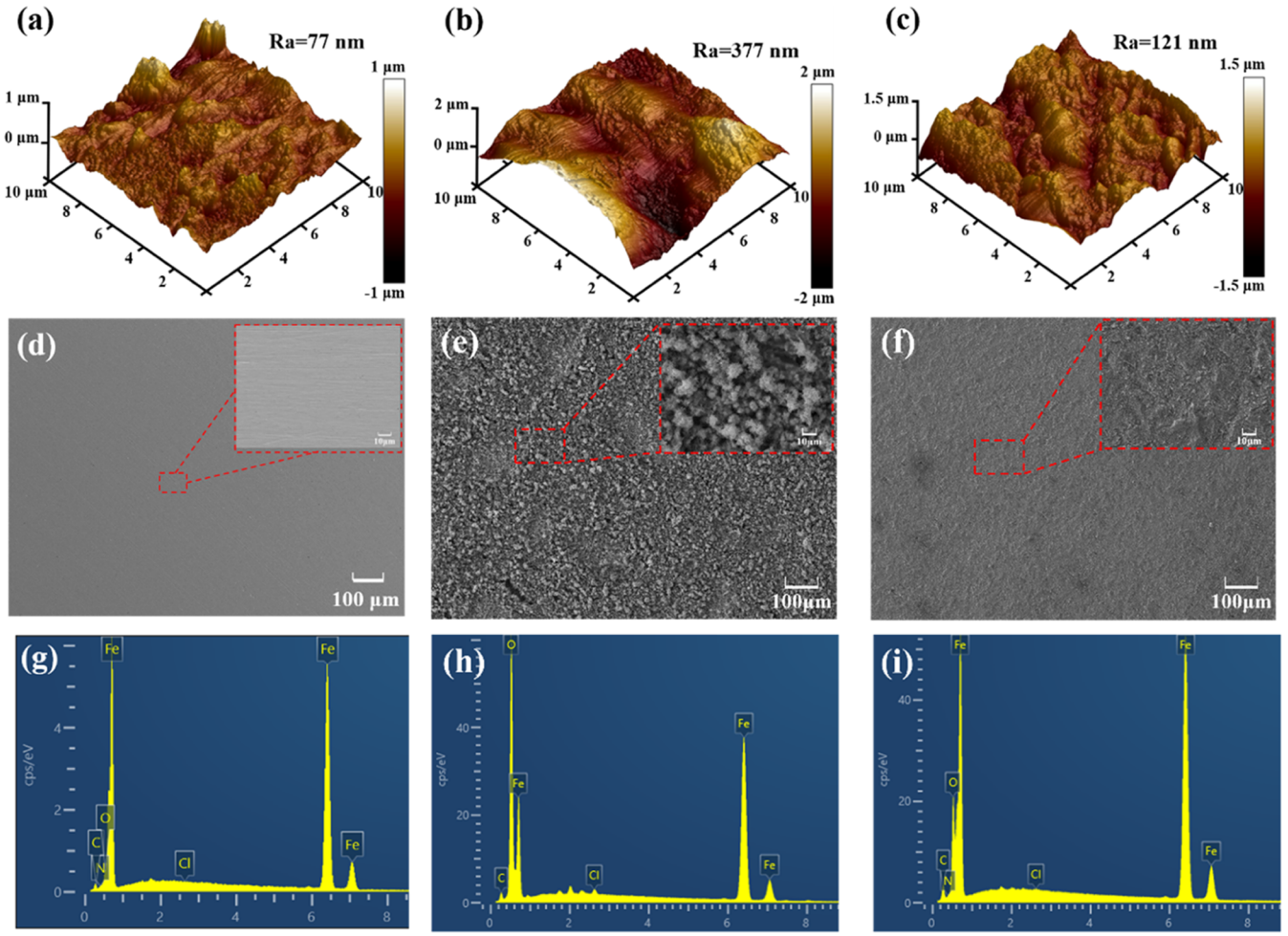

Figure 6. (a–c) AFM images of Q235 carbon steel in different states; (d–f, g–i) SEM and EDS images of Q235 carbon steel in different states.

different states was analyzed by an energy-dispersive spectrometer. As can be seen from Figures 6g–i and S5 and Table S2, the main components of the Q235 carbon steel sample are C and Fe elements. Compared with the original Q235 carbon steel (Figure 6g), after soaking in 1 M HCl solution for 24 h (Figure 6h), the content of Fe atoms on the surface of Q235 carbon steel decreased from 85.15 to 42.5%, while the content of O increased from 2.82 to 47%, Cl atoms appeared on the surface, and serious corrosion occurred on the surface metal. By comparing the EDS data of Q235 samples in the HCl solution without ZCQDs and HCl solution with ZCQDs, it can be obviously seen that the atomic content of Fe on the metal surface increases after the addition of ZCQDs, while the atomic content of O decreases sharply (Figure 6h,6i). This is due to the accumulation of ZCQDs on the surface of Q235 carbon steel to form a dense protective film through physical and chemical adsorption and agglomeration, which inhibits the dissolution of HCl on the steel.[10] At the same time, EDS data show that after adding ZCQDs, the content of O atoms and C atoms on the metal surface increased compared with the original Q235 sample because ZCQDs were obtained through pyrolysis oxidation (XPS data confirmed that ZCQDs contain a large amount of oxygen, and its main components are C and O). This phenomenon is similar to EDS analysis of carbon point corrosion inhibitor produced by chemical oxidation after forming a film on the metal surface.[56] These results also show that ZCQDs form a dense and thick protective film on the metal surface. It should be noted that it is difficult for EDS to detect ZCQDs effectively due to their low N atom content (2.36% recorded by XPS).[49]

3.5. Inhibition Mechanism for ZCQDs. First, data such as FTIR and XPS in Figure 3 show that ZCQDs contain the O and N functional groups, and the ζ-potential of ZCQDs in 1 M HCl solution is +26.18 mV. Combined with electrochemical data and surface analysis results, it can be inferred that the protective film of ZCQDs on the metal surface is formed through the combined action of physical adsorption and chemical adsorption. When ZCQDs are added to 1 M HCl solution, the paired electrons and the lone electron pairs in the nitrogen atoms were transferred to vacant d-orbitals of iron, and rigid covalent bonds were formed through p-electron transfer. Graphitic N is responsible for physical adsorption, while chemisorption is carried out through the pyridine and pyrrole-like N atoms.[11,14] Physical adsorption is mainly due to the electrostatic action of hydroxyl, carbonyl, and amide functional groups in ZCQDs, so that ZCQDs are combined with Cl^- in solution, and then Cl^- is combined with carbon steel as a connecting bridge to form a physical adsorption film.[49] The R–P adsorption isotherm data (Figure 5) also show that the adsorption of ZCQDs on the metal surface includes physical and chemical adsorption. Subsequently, on the formed adsorption film, ZCQDs will form a thicker and denser protective film due to their own agglomeration and Cl^- bridging action. The analysis of EIS data shows that the

https://doi.org/10.1021/acsomega.3c06702
ACS Omega 2023, 8, 46934–46945

thickness and density of the protective film formed by ZCQDs increased with the increase of the addition amount, which was consistent with the results of the above judgment. The potentiodynamic polarization curve (Figure 4f) shows that ZCQDs, as a corrosion inhibitor for carbon steel in an acidic environment, are mainly protective of the cathode, although it is a mixed corrosion inhibitor. The experimental data of weight loss experiment, EIS experiment, and PDP experiment are in good agreement, and their results all show that when the concentration of ZCQDs in the solution reaches 100 mg/L, the corrosion inhibition rate is close to or more than 90% and then continue to increase the concentration of ZCQDs and when the concentration reaches 200 mg/L, the corrosion inhibition rate will come to near 95%. From the data of the weight loss experiments, EIS, and PDP, it can be seen that when the concentration exceeds 100 mg/L, the rate of corrosion inhibition increases slowly. By analyzing the test data and combining with the adsorption behavior of ZCQDs on the metal surface, it is not difficult to find that this phenomenon is due to the slow diffusion of ZCQDs at low concentrations, small adsorption accumulation, and the formed protective film is not dense enough and the thickness is small. When the concentration reaches 100 mg/L, the adsorption film formed by ZCQDs on the metal surface can almost completely cover the metal surface, and the ZCQDs accumulated on the surface of the adsorption film due to the agglomeration effect can reach a near dynamic equilibrium state, fill the gap, and increase the thickness, so that ZCQDs have a good corrosion inhibition performance. AFM, SEM, and EDS (Figure 6) prove the existence and state of the membrane, which is consistent with the above analysis results. Based on the above analysis results, we proposed the corrosion inhibition mechanism model of ZCQDs as shown in Figure 7 to explain the corrosion

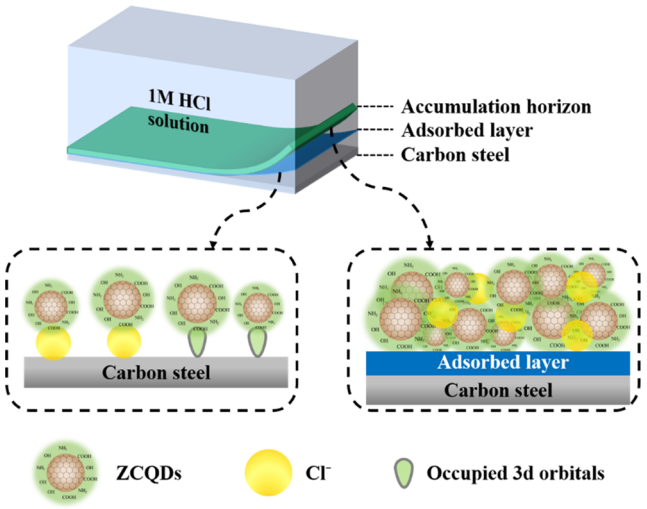

Figure 7. Inhibition Mechanism of ZCQDs for Q235 carbon steel in the HCl solution.

inhibition behavior of ZCQDs on Q235 carbon steel in a 1 M HCl solution. As shown in Figure 7, ZCQDs first form a protective film through physical adsorption and chemisorption and then accumulate more ZCQDs on the protective film formed by adsorption, forming a thicker and denser protective film to protect the metal.

4. CONCLUSIONS

The corrosion inhibition mechanism of ZCQDs on Q235 carbon steel in 1 M HCl solution was analyzed by the characterization of ZCQDs, corrosion inhibition performance test, and metal surface analysis. Here's what we learned:

(1) ZCQDs can be used as a corrosion inhibitor for Q235 carbon steel in 1 M HCl solution, and its corrosion inhibition rate is proportional to the concentration. When the concentration is 200 mg/L, the best corrosion inhibition rate can reach 95.98%, When the dosage reaches 200 mg/L, the IE_{EIS} value reaches 95.98%, and at this concentration, effective protection of at least 132h (IE > 90%) is provided.

(2) ZCQDs is a mixed-type corrosion inhibitor for carbon steel in an acidic medium, but its main protection is the cathode.

(3) The adsorption of ZCQDs on the metal surface follows the R−P adsorption isotherm model, involving both chemisorption and physisorption.

(4) The corrosion inhibition performance analysis is in good agreement with the metal surface analysis, which indicates that ZCQDs can form a thick and dense protective layer on the metal surface.

■ ASSOCIATED CONTENT

Supporting Information

The Supporting Information is available free of charge at https://pubs.acs.org/doi/10.1021/acsomega.3c06702.

In Supporting Information, we provide the data obtained by analyzing the lattice spacing of ZCQDs with GMS 3 software, the full spectrum of XPS data, and the long-acting test data of ZCQDs in 1 M HCl solution. Fitundluich and Langmuir isotherm fit data were used, as well as EDS data for metal surfaces (PDF)

■ AUTHOR INFORMATION

Corresponding Author

Xuemei Ma − *School of Chemistry and Chemical Engineering, North University of China, Taiyuan 030051, China;* orcid.org/0000-0002-0813-0454; Email: maxuemei@nuc.edu.cn

Authors

Liming Dong − *School of Chemistry and Chemical Engineering, North University of China, Taiyuan 030051, China*

Yuyue Ma − *School of Chemistry and Chemical Engineering, North University of China, Taiyuan 030051, China*

Xiaohan Jin − *College of Chemistry and Chemical Engineering, China University of Petroleum (East China), Qingdao 266580, China*

Li Feng − *School of Chemistry and Chemical Engineering, North University of China, Taiyuan 030051, China*

Hailin Zhu − *School of Chemistry and Chemical Engineering, North University of China, Taiyuan 030051, China*

Zhiyong Hu − *School of Chemistry and Chemical Engineering, North University of China, Taiyuan 030051, China*

Complete contact information is available at: https://pubs.acs.org/10.1021/acsomega.3c06702

Author Contributions

L.D.: Conceptualization, validation, writing—original draft, writing—review and editing. Y.M.: Data curation. X.J.: Methodology. L.F.: Data curation and validation. H.Z.: Investigation. Z.H.: Supervision and project administration. X.M.: Conceptualization, methodology, writing—original draft, and writing—review and editing.

Notes

The authors declare no competing financial interest.

■ ACKNOWLEDGMENTS

The authors appreciate financial support from the Research Project Supported by Shanxi Scholarship Council of China (No. 2022-137) and Shanxi Graduate Education Innovation Project (2022Y619).

■ REFERENCES

(1) Ahamad, I.; Prasad, R.; Quraishi, M. A. Thermodynamic, Electrochemical and Quantum Chemical Investigation of Some Schiff Bases as Corrosion Inhibitors for Mild Steel in Hydrochloric Acid Solutions. *Corros. Sci.* **2010**, *52* (3), 933−942.

(2) Quadri, T. W.; Olasunkanmi, L. O.; Akpan, E. D.; Alfantazi, A.; Obot, I. B.; Verma, C.; Al-Mohaimeed, A. M.; Ebenso, E. E.; Quraishi, M. A. Chromeno-Carbonitriles as Corrosion Inhibitors for Mild Steel in Acidic Solution: Electrochemical, Surface and Computational Studies. *RSC Adv.* **2021**, *11* (4), 2462−2475.

(3) Bedair, M. A.; El-Sabbah, M. M. B.; Fouda, A. S.; Elaryian, H. M. Synthesis, Electrochemical and Quantum Chemical Studies of Some Prepared Surfactants Based on Azodye and Schiff Base as Corrosion Inhibitors for Steel in Acid Medium. *Corros. Sci.* **2017**, *128*, 54−72.

(4) Hu, Z.; Meng, Y.; Ma, X.; Zhu, H.; Li, J.; Li, C.; Cao, D. Experimental and Theoretical Studies of Benzothiazole Derivatives as Corrosion Inhibitors for Carbon Steel in 1 M HCl. *Corros. Sci.* **2016**, *112*, 563−575.

(5) Natarajan, R.; Al Shibli, F. S. Z. S. Synthesis of Biomass Derived Product from Ziziphus Spina-Christi and Application for Surface Protection of Metal under Acidic Environment- Performance Evaluation and Thermodynamic Studies. *Chemosphere* **2021**, *284*, No. 131375.

(6) Munawaroh, H. S. H.; Sunarya, Y.; Anwar, B.; Priatna, E.; Risa, H.; Koyande, A. K.; Show, P.-L. Protoporphyrin Extracted from Biomass Waste as Sustainable Corrosion Inhibitors of T22 Carbon Steel in Acidic Environments. *Sustainability* **2022**, *14* (6), 3622.

(7) Wang, X.; Feng, Y.; Dong, P.; Huang, J. A Mini Review on Carbon Quantum Dots: Preparation, Properties, and Electrocatalytic Application. *Front. Chem.* **2019**, *7*, 671.

(8) Tian, L.; Li, Z.; Wang, P.; Zhai, X.; Wang, X.; Li, T. Carbon Quantum Dots for Advanced Electrocatalysis. *J. Energy Chem.* **2021**, *55*, 279−294.

(9) Cui, M.; Ren, S.; Xue, Q.; Zhao, H.; Wang, L. Carbon Dots as New Eco-Friendly and Effective Corrosion Inhibitor. *J. Alloys Compd.* **2017**, *726*, 680−692.

(10) Zhu, M.; He, Z.; Guo, L.; Zhang, R.; Anadebe, V. C.; Obot, I. B.; Zheng, X. Corrosion Inhibition of Eco-Friendly Nitrogen-Doped Carbon Dots for Carbon Steel in Acidic Media: Performance and Mechanism Investigation. *J. Mol. Liq.* **2021**, *342*, No. 117583.

(11) Ye, Y.; Yang, D.; Chen, H.; Guo, S.; Yang, Q.; Chen, L.; Zhao, H.; Wang, L. A High-Efficiency Corrosion Inhibitor of N-Doped Citric Acid-Based Carbon Dots for Mild Steel in Hydrochloric Acid Environment. *J. Hazard. Mater.* **2020**, *381*, No. 121019.

(12) Cao, S.; Liu, D.; Wang, T.; Ma, A.; Liu, C.; Zhuang, X.; Ding, H.; Mamba, B. B.; Gui, J. Nitrogen-Doped Carbon Dots as High-Effective Inhibitors for Carbon Steel in Acidic Medium. *Colloids Surf., A* **2021**, *616*, No. 126280.

(13) Cui, M.; Ren, S.; Zhao, H.; Wang, L.; Xue, Q. Novel Nitrogen Doped Carbon Dots for Corrosion Inhibition of Carbon Steel in 1 M HCl Solution. *Appl. Surf. Sci.* **2018**, *443*, 145−156.

(14) Liu, Z.; Ye, Y. W.; Chen, H. Corrosion Inhibition Behavior and Mechanism of N-Doped Carbon Dots for Metal in Acid Environment. *J. Cleaner Prod.* **2020**, *270*, No. 122458.

(15) Luo, J.; Cheng, X.; Zhong, C.; Chen, X.; Ye, Y. W.; Zhao, H.; Chen, H. Effect of Reaction Parameters on the Corrosion Inhibition Behavior of N-Doped Carbon Dots for Metal in 1 M HCl Solution. *J. Mol. Liq.* **2021**, *338*, No. 116783.

(16) Pan, L.; Li, G.; Wang, Z.; Liu, D.; Zhu, W.; Tong, C.; Zhu, R.; Hu, S. Carbon Dots as Environment-Friendly and Efficient Corrosion Inhibitors for Q235 Steel in 1 M HCl. *Langmuir* **2021**, *37* (49), 14336−14344.

(17) Yang, D.; Ye, Y.; Su, Y.; Liu, S.; Gong, D.; Zhao, H. Functionalization of Citric Acid-Based Carbon Dots by Imidazole toward Novel Green Corrosion Inhibitor for Carbon Steel. *J. Cleaner Prod.* **2019**, *229*, 180−192.

(18) Luo, J.; Cheng, X.; Chen, X.; Zhong, C. F.; Xie, H.; Ye, Y. W.; Zhao, H. C.; Li, Y.; Chen, H. The Effect of N and S Ratios in N, S Co-Doped Carbon Dot Inhibitor on Metal Protection in 1 M HCl Solution. *J. Taiwan Inst. Chem. Eng.* **2021**, *127*, 387−398.

(19) Guo, T.; et al. Two New Phenolic Glycosides from the Stem of Zanthoxylum Armatum DC. *Nat. Prod. Res.* **2017**, *31*, 2335−2340, DOI: 10.1080/14786419.2017.1303695.

(20) Li, L.; Wu, H.; Liu, S.; et al. Chemical Constituents from the Leaves of Zanthoxylum Nitidum (Roxb.) DC. *Biochem. Syst. Ecol.* **2020**, *91*, No. 104080, DOI: 10.1016/j.bse.2020.104080.

(21) Quraishi, M. A.; Chauhan, D. S.; Saji, V. S.; et al. Heterocyclic Biomolecules as Green Corrosion Inhibitors. *J. Mol. Liq.* **2021**, *341*, No. 117265, DOI: 10.1016/j.molliq.2021.117265.

(22) Ma, C.; Yin, C.; Fan, Y.; Yang, X.; Zhou, X. Highly Efficient Synthesis of N-Doped Carbon Dots with Excellent Stability through Pyrolysis Method. *J. Mater. Sci.* **2019**, *54* (13), 9372−9384.

(23) Wang, J.; Jing, J.; Feng, L.; Zhu, H.; Hu, Z.; Ma, X. Study on Corrosion Inhibition Behavior and Adsorption Mechanism of Novel Synthetic Surfactants for Carbon Steel in 1 M HCl Solution. *Sustainable Chem. Pharm.* **2021**, *23*, No. 100500.

(24) Jin, X.; Wang, J.; Zheng, S.; Li, J.; Ma, X.; Feng, L.; Zhu, H.; Hu, Z. The Study of Surface Activity and Anti-Corrosion of Novel Surfactants for Carbon Steel in 1 M HCl. *J. Mol. Liq.* **2022**, *353*, No. 118747.

(25) Cen, H.; Zhang, X.; Zhao, L.; Chen, Z.; Guo, X. Carbon Dots as Effective Corrosion Inhibitor for 5052 Aluminium Alloy in 0.1 M HCl Solution. *Corros. Sci.* **2019**, *161*, No. 108197.

(26) Zhu, M.; Guo, L.; He, Z.; Marzouki, R.; Zhang, R.; Berdimurodov, E. Insights into the Newly Synthesized N-Doped Carbon Dots for Q235 Steel Corrosion Retardation in Acidizing Media: A Detailed Multidimensional Study. *J. Colloid Interface Sci.* **2022**, *608*, 2039−2049.

(27) Sarkar, T. K.; Saraswat, V.; Mitra, R. K.; Obot, I. B.; Yadav, M. Mitigation of Corrosion in Petroleum Oil Well/Tubing Steel Using Pyrimidines as Efficient Corrosion Inhibitor: Experimental and Theoretical Investigation. *Mater. Today Commun.* **2021**, *26*, No. 101862.

(28) Cen, H.; Cao, J.; Chen, Z. Functionalized Carbon Nanotubes as a Novel Inhibitor to Enhance the Anticorrosion Performance of Carbon Steel in CO2-Saturated NaCl Solution. *Corros. Sci.* **2020**, *177*, No. 109011.

(29) Li, W.; Liu, Y.; Wang, B.; Song, H.; Liu, Z.; Lu, S.; Yang, B. Kilogram-Scale Synthesis of Carbon Quantum Dots for Hydrogen Evolution, Sensing and Bioimaging. *Chin. Chem. Lett.* **2019**, *30* (12), 2323−2327.

(30) Miao, X.; Qu, D.; Yang, D.; Nie, B.; Zhao, Y.; Fan, H.; Sun, Z. Synthesis of Carbon Dots with Multiple Color Emission by Controlled Graphitization and Surface Functionalization. *Adv. Mater.* **2018**, *30* (1), No. 1704740.

(31) Arumugham, T.; Alagumuthu, M.; Amimodu, R. G.; Munusamy, S.; Iyer, S. K. A Sustainable Synthesis of Green Carbon Quantum Dot (CQD) from Catharanthus Roseus (White Flowering Plant) Leaves and Investigation of Its Dual Fluorescence Responsive Behavior in Multi-Ion Detection and Biological Applications.

https://doi.org/10.1021/acsomega.3c06702
ACS Omega 2023, 8, 46934−46945

Sustainable Mater. Technol. **2020**, *23*, No. e00138, DOI: 10.1016/j.susmat.2019.e00138.
(32) Liu, J.; Geng, Y.; Li, D.; Yao, H.; Huo, Z.; Li, Y.; Zhang, K.; Zhu, S.; Wei, H.; Xu, W.; Jiang, J.; Yang, B. Deep Red Emissive Carbonized Polymer Dots with Unprecedented Narrow Full Width at Half Maximum. *Adv. Mater.* **2020**, *32* (17), No. 1906641.
(33) Ouakki, M.; Galai, M.; Rbaa, M.; Abousalem, A. S.; Lakhrissi, B.; Rifi, E. H.; Cherkaoui, M. Investigation of Imidazole Derivatives as Corrosion Inhibitors for Mild Steel in Sulfuric Acidic Environment: Experimental and Theoretical Studies. *Ionics* **2020**, *26* (10), 5251−5272.
(34) Cen, H.; Chen, Z.; Guo, X. N, S Co-Doped Carbon Dots as Effective Corrosion Inhibitor for Carbon Steel in CO2-Saturated 3.5% NaCl Solution. *J. Taiwan Inst. Chem. Eng.* **2019**, *99*, 224−238.
(35) Mobin, M.; Zehra, S.; Aslam, R. L-Phenylalanine Methyl Ester Hydrochloride as a Green Corrosion Inhibitor for Mild Steel in Hydrochloric Acid Solution and the Effect of Surfactant Additive. *RSC Adv.* **2016**, *6* (7), 5890−5902.
(36) Porcayo-Calderon, J.; de la Escalera, L. M. M.; Canto, J.; Casales-Diaz, M. Imidazoline Derivatives Based on Coffee Oil as CO2 Corrosion Inhibitor. *Int. J. Electrochem. Sci.* **2015**, *10* (4), 3160−3176.
(37) Usman, B. J.; Gasem, Z. M.; Umoren, S. A.; Solomon, M. M. Eco-Friendly 2-Thiobarbituric Acid as a Corrosion Inhibitor for API 5L X60 Steel in Simulated Sweet Oilfield Environment: Electrochemical and Surface Analysis Studies. *Sci. Rep.* **2019**, *9* (1), No. 830.
(38) Zhu, M.; Rao, S.; He, Z.; Hu, J.; Xiong, L.; Zhang, R.; Han, S.; Li, L. Tribological Properties of Dithiocarbamate Triazine and Its Competitive Adsorption Behavior Compared to T701 on the Corrosion Inhibition of Q235 Steel. *Surf. Topogr. Metrol. Prop.* **2021**, *9* (1), No. 015003.
(39) Qiang, Y.; Zhang, S.; Zhao, H.; Tan, B.; Wang, L. Enhanced Anticorrosion Performance of Copper by Novel N-Doped Carbon Dots. *Corros. Sci.* **2019**, *161*, No. 108193.
(40) Tan, J.; Guo, L.; Yang, H.; Zhang, F.; El Bakri, Y. Synergistic Effect of Potassium Iodide and Sodium Dodecyl Sulfonate on the Corrosion Inhibition of Carbon Steel in HCl Medium: A Combined Experimental and Theoretical Investigation. *RSC Adv.* **2020**, *10* (26), 15163−15170.
(41) Behpour, M.; Ghoreishi, S. M.; Soltani, N.; Salavati-Niasari, M. The Inhibitive Effect of Some Bis-N,S-Bidentate Schiff Bases on Corrosion Behaviour of 304 Stainless Steel in Hydrochloric Acid Solution. *Corros. Sci.* **2009**, *51* (5), 1073−1082.
(42) Zeng, X.; et al. Three Imidazole Ionic Liquids as Green and Eco-Friendly Corrosion Inhibitors for Mild Steel in Sulfuric Acid Medium. *J. Mol. Liq.* **2021**, *324*, No. 115063, DOI: 10.1016/j.molliq.2020.115063.
(43) Cui, R.; Gu, N.; Li, C. Polyaspartic Acid as a Green Corrosion Inhibitor for Carbon Steel. *Mater. Corros.* **2011**, *62* (4), 362−369.
(44) Keramatinia, M.; Ramezanzadeh, M.; Bahlakeh, G.; Ramezanzadeh, B. Synthesis of a Multi-Functional Zinc-Centered Nitrogen-Rich Graphene-like Thin Film from Natural Sources on the Steel Surface for Achieving Superior Anti-Corrosion Properties. *Corros. Sci.* **2021**, *178*, No. 109077.
(45) Satpati, S.; Suhasaria, A.; Ghosal, S.; Adhikari, U.; Banerjee, P.; Dey, S.; Sukul, D. Anti-Corrosive Propensity of Naturally Occurring Aldehydes and 1-(3-Aminopropyl)Imidazole Condensed Schiff Bases: Comparison on the Effect of Extended Conjugation over Electron Donating Substituents. *J. Mol. Struct.* **2022**, *1268*, No. 133684.
(46) Zhao, H.; Sun, T.-Y.; Huang, L.-F.; Wei, J.; Qiu, S. A Green Strategy for Nitrogen-Doped Polymer Nanodots with High Oxygen and Chloride Corrosion Resistance in Extremely Acidic Condition. *Chem. Eng. J.* **2022**, *437*, No. 135242.
(47) Okafor, P. C.; Liu, X.; Zheng, Y. G. Corrosion Inhibition of Mild Steel by Ethylamino Imidazoline Derivative in CO2-Saturated Solution. *Corros. Sci.* **2009**, *51* (4), 761−768.
(48) Khaled, K. F. The Inhibition of Benzimidazole Derivatives on Corrosion of Iron in 1 M HCl Solutions. *Electrochim. Acta* **2003**, *48* (17), 2493−2503.
(49) Long, W.-J.; Li, X.-Q.; Yu, Y.; He, C. Green Synthesis of Biomass-Derived Carbon Dots as an Efficient Corrosion Inhibitor. *J. Mol. Liq.* **2022**, *360*, No. 119522.
(50) Al-Ghouti, M. A.; Da'ana, D. A. Guidelines for the Use and Interpretation of Adsorption Isotherm Models: A Review. *J. Hazard. Mater.* **2020**, *393*, No. 122383.
(51) Ogunleye, O. O.; Arinkoola, A. O.; Eletta, O. A.; Agbede, O. O.; Osho, Y. A.; Morakinyo, A. F.; Hamed, J. O. Green Corrosion Inhibition and Adsorption Characteristics of Luffa Cylindrica Leaf Extract on Mild Steel in Hydrochloric Acid Environment. *Heliyon* **2020**, *6* (1), No. e03205.
(52) Wu, F.-C.; Liu, B.-L.; Wu, K.-T.; Tseng, R.-L. A New Linear Form Analysis of Redlich−Peterson Isotherm Equation for the Adsorptions of Dyes. *Chem. Eng. J.* **2010**, *162* (1), 21−27.
(53) Mishra, P. K.; Gahlyan, P.; Kumar, R.; Rai, P. K. Aero-Gel Based Cerium Doped Iron Oxide Solid Solution for Ultrafast Removal of Arsenic. *ACS Sustainable Chem. Eng.* **2018**, *6* (8), 10668−10678.
(54) Li, X.; Deng, S.; Fu, H.; Mu, G. Synergistic Inhibition Effect of Rare Earth Cerium(IV) Ion and Anionic Surfactant on the Corrosion of Cold Rolled Steel in H2SO4 Solution. *Corros. Sci.* **2008**, *50* (9), 2635−2645.
(55) Zhou, L.; Li, A.; Ma, F.; Zhao, H.; Deng, F.; Pi, S.; Tang, A.; Yang, J. Combining High Electron Transfer Efficiency and Oxidation Resistance in nZVI with Coatings of Microbial Extracellular Polymeric Substances to Enhance Sb(V) Reduction and Adsorption. *Chem. Eng. J.* **2020**, *395*, No. 125168.
(56) Zhu, J.; Zhu, M.; He, Z.; Xiong, L.; Zhang, R.; Guo, L. Chemical Oxidation Synthesized High-Yield Carbon Dots for Acid Corrosion Inhibition of Q235 Steel. *ChemistrySelect* **2023**, *8* (7), No. e202204621.

https://doi.org/10.1021/acsomega.3c06702
ACS Omega 2023, 8, 46934−46945